Science of the Total Environment 778 (2021) 146265

Contents lists available at ScienceDirect

Science of the Total Environment

journal homepage: www.elsevier.com/locate/scitotenv

Formation of peroxyacetyl nitrate (PAN) and its impact on ozone production in the coastal atmosphere of Qingdao, North China

Yuhong Liu [a], Hengqing Shen [a,*], Jiangshan Mu [a], Hongyong Li [a], Tianshu Chen [a], Juan Yang [a], Ying Jiang [a], Yujiao Zhu [a], He Meng [b], Can Dong [a], Wenxing Wang [a], Likun Xue [a,c,**]

[a] Environment Research Institute, Shandong University, Qingdao, Shandong 266237, China
[b] Qingdao Eco-environment Monitoring Center of Shandong Province, Qingdao, Shandong 266003, China
[c] Ji'nan Eco-Environmental Monitoring Center of Shandong Province, Ji'nan, Shandong 250000, China

HIGHLIGHTS

- PAN was measured in the coastal atmosphere of Qingdao in both autumn and summer.
- Sensitivities of PAN to precursors and the differences from O_3 were explored.
- PAN could promote or suppress O_3 production by affecting radical cycling.

GRAPHICAL ABSTRACT

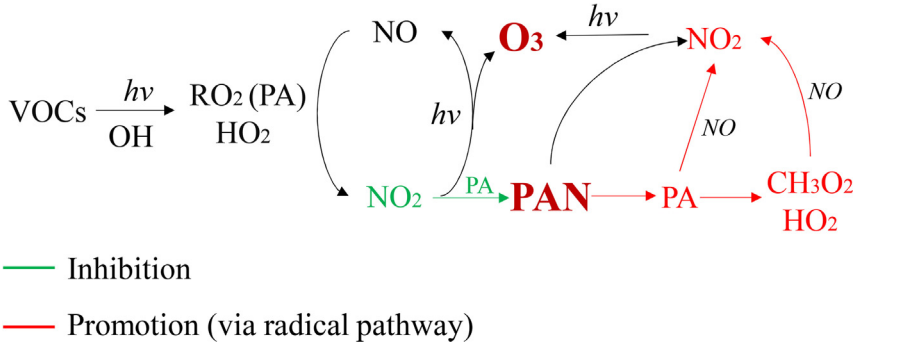

ARTICLE INFO

Article history:
Received 23 November 2020
Received in revised form 8 February 2021
Accepted 28 February 2021
Available online 8 March 2021

Editor: Pingqing Fu

Keywords:
PAN
Ozone
Coastal atmosphere
VOCs
Observation-based model

ABSTRACT

Peroxyacetyl nitrate (PAN), acting as a relatively long-lived reservoir for both NO_x and radicals, plays a crucial role in ozone (O_3) formation in the troposphere. However, its quantitative impacts on radical concentrations and O_3 production were rarely studied in the coastal atmosphere. In this study, ambient concentrations of PAN, O_3, and related species were simultaneously measured from October 5 to November 10, 2018 (autumn), and July 14 to August 24, 2019 (summer) at a rural coastal site in Qingdao, North China. The formation mechanism of PAN and its impact on in-situ O_3 production were explored with an observation-based chemical box model. Photochemical formation of PAN and O_3 was controlled by both NO_x and VOCs, and acetaldehyde and methylglyoxal were the main contributors to PAN formation. However, the sensitivities of PAN to precursors were larger than that of O_3 in autumn while smaller in summer, which was mainly caused by the rapid decomposition of PAN at high temperatures. Zero-out sensitivity simulation showed that PAN could either promote or inhibit the in-situ O_3 formation by affecting the radical chemistry. It tended to suppress O_3 production by competing with precursors and terminating radical chain reactions under low-NO_x and low-RO_x circumstances but enhanced O_3 production by supplying RO_2 radicals under conditions with sufficient NO_x. This study provides some new complementary insights into the formation mechanism of PAN and its impacts on O_3 production, and has implications for the formulation of control policy to mitigate regional photochemical pollution in northern China.

* Corresponding author.
** Correspondence to: L. Xue, Ji'nan Eco-Environmental Monitoring Center of Shandong Province, Ji'nan, Shandong 250000, China.
E-mail addresses: hqshen@sdu.edu.cn (H. Shen), xuelikun@sdu.edu.cn (L. Xue).

https://doi.org/10.1016/j.scitotenv.2021.146265
0048-9697/

1. Introduction

Peroxyacetyl nitrate ($CH_3C(O)O_2NO_2$, PAN) is formed alongside ozone (O_3) from photochemical reactions of volatile organic compounds (VOCs) and nitrogen oxides ($NO_x = NO+NO_2$) (Aikin et al., 1982; Lonneman et al., 1976), and has long been regarded as a photochemical pollution indicator (Penkett and Brice, 1986; Stephens, 1969). Despite relatively low atmospheric concentrations compared with O_3, usually with a few pptv in remote regions (Mills et al., 2007; Stephens et al., 1956) to several ppbv in polluted urban areas (Lee et al., 2008; Xue et al., 2014a; Zhang et al., 2019b; Zhang et al., 2014), its overall bio-toxic effect is even one or two orders of magnitude greater (Temple and Taylor, 1983).

The exclusive formation pathway of PAN is the termination reaction of peroxyacetyl radical ($CH_3C(O)O_2$, PA) with NO_2 (R2). Unlike almost all reactive VOCs involved in the generation of O_3, only VOCs that produce PA radical can generate PAN (R1) (LaFranchi et al., 2009; Xue et al., 2014a). The dominant sources of PA radical are oxidation or photolysis of a subset of oxygenated VOCs (OVOCs), such as acetaldehyde, acetone, and methylglyoxal (Zhang et al., 2015). A large proportion of these precursors are produced from the oxidation of primarily emitted VOCs, such as ethane, propene, isoprene, and aromatics (Qian et al., 2019; Xue et al., 2014a). The relative importance of PA radical precursors is highly variable in different environments depending on the composition and concentrations of VOCs and NO_x (LaFranchi et al., 2009; Xue et al., 2014a; Zeng et al., 2019).

$$\mathrm{VOCs} + \mathrm{hv/OH/O_3/NO_3} \xrightarrow{O_2} CH_3C(O)O_2 \quad (R1)$$

$$CH_3C(O)O_2 + NO_2 \rightarrow CH_3C(O)O_2NO_2 \quad (R2)$$

$$CH_3C(O)O_2NO_2 \rightarrow CH_3C(O)O_2 + NO_2 \quad (R3)$$

$$CH_3C(O)O_2 + NO \rightarrow CH_3O_2 + NO_2 \quad (R4)$$

$$CH_3C(O)O_2 + HO_2/RO_2 \rightarrow \mathrm{products} \quad (R5)$$

PAN plays a crucial role in the complex radical chemistry and O_3 formation of the troposphere, acting as a relatively long-lived reservoir for both NO_x and organic radicals (Crowley et al., 2018; LaFranchi et al., 2009). PAN is thermally unstable in the boundary layer; its lifetime against thermal decomposition is about only 2 h at a typical NO_2/NO ratio of ~7 and the ambient temperature of 25 °C (R3). However, it increases rapidly with the decrease of temperature, approximately five times every 10 °C, leading to a lifetime of over a month in the mid-troposphere (Atkinson et al., 2006). This property makes it the principal reservoir for short-lived NO_x, facilitating the transport and release of NO_x to remote regions, with significant implications for global O_3 distribution (Fischer et al., 2010; Singh and Hanst, 1981).

The promotion of PAN decomposition on remote O_3 production via the release of NO_x under low NO_x conditions has been discussed extensively (Jiang et al., 2016; Penkett and Brice, 1986). However, evaluations of its impact on radical chemistry and subsequent O_3 formation via acting as a temporary sink or source of PA radical are scarce. PA radical is one of the four most abundant organic peroxy radicals in the troposphere (Tyndall et al., 2001). In addition to reacting with NO_2 to form PAN (temporary sink), it can also react with NO, HO_2, and RO_2 (permanent loss, R4 and R5), producing various products, e.g., HCHO, $CH_3C(O)O_2H$, and CH_3O_2 radical (Fischer et al., 2014; Zhang et al., 2010). These permanent loss channels of PA radical may be significant under some conditions (Wolfe et al., 2014; Zeng et al., 2019), which would affect the distribution of atmospheric radicals and the sensitivities of O_3 and PAN formation to their precursors. Recently, Zeng et al. (2019) found that the O_3 production rate was weakened by 36% by PAN photochemistry in a VOC-limited suburb of Hong Kong, possibly due to its "weakening effect" on radical concentration. However, PAN could also reserve as a temporary sink for NO_x, slowing the removal rate of NO_2 by OH and extending the radical chain length, and thus it should promote O_3 production. These imply that the impact of PAN on O_3 production may be highly dependent on environmental conditions and requires more detailed evaluations.

The coastal area of Qingdao is affected by both clean marine air masses and polluted continental air masses (Yang et al., 2021), and would be an ideal place to study PAN formation and its implication on O_3 production under contrast environmental conditions. In this study, two intensive field campaigns were conducted in a coastal area of Qingdao in autumn 2018 and summer 2019, and a suite of chemical species, including PAN, O_3, and their precursors, were simultaneously measured. With the aid of an observation-based box model, the photochemical formation of PAN and the sensitivity differences of PAN and O_3 to their precursors were examined. More importantly, both promotion and inhibition effects of PAN on O_3 production were observed, and the corresponding changes of RO_x (OH, HO_2, and RO_2) in different scenarios were discussed. This study provides new complementary insights into the formation of PAN and its impact on O_3 production via the pathway of radical chemistry.

2. Methods

2.1. Observation site

The sampling location is at a rural coastal site of Qingdao, north China. The site is over 20 km away from the nearest urban areas (Jimo district of Qingdao) and separated from Qingdao downtown by Mountain Lao of 1130 m above sea level (Fig. 1). The instruments were located on a third-floor roof of the Gan Chang building in the Qingdao campus of Shandong University, 8 m above the ground. About 500 m to the east and the west of the sampling site are the sea and a national highway, respectively. There are no significant industrial sources nearby. More details of the study site can be found elsewhere (Yang et al., 2021). The two field campaigns were conducted from October 5 to November 10 (autumn), 2018, and July 14 to August 24 (summer), 2019, respectively. Field measurements were carried out in summer and autumn, both of which are typical photochemical pollution season with distinct air mass transport patterns under the influence of the East Asian monsoon.

2.2. Measurement techniques

PAN was measured with a commercially available automatic PAN-Analyzer equipped with gas chromatography (GC) and electron capture detector (ECD) (*PAN1510A, Beijing Convenient Environmental Tech Co. Ltd, China*), and the sampling time resolution was 10 min. This analytical method has been used extensively for PAN measurements (Zhang et al., 2012). This instrument measured the concentrations of CCl_4 simultaneously, and its minimal variation indicated the stability of the instrument. The calibrations were performed every two weeks by injecting known concentrations of standard gases of PAN and CCl_4. The standard gas of PAN was generated by the UV irradiation (254 nm) of a gaseous mixture of excess acetone and NO, and the CCl_4 standard gas was purchased from the National Institute of Metrology. The detection limits of the GC-ECD (three times the signal to noise) for PAN and CCl_4 were 22 pptv and 5 pptv, respectively. The carrier gas was changed to high purity helium to enhance the stability of the instrument.

The concentrations of VOCs were monitored by online gas chromatography–mass spectrometry (*TT24xr, Makers, UK; GC–MS, Thermo Scientific, USA*). The instrument system can quantitatively analyze 106 VOCs in the ambient atmosphere, including 29 alkanes, 11 alkenes, one alkyne, 17 aromatics, 35 halogenated hydrocarbons, and 13 OVOCs. This system automatically collected air samples for 1 h at a 10 mL min^{-1} flow rate. The VOCs were absorbed and collected by the adsorbent in the cold trap, then sent into the analysis system through rapid heating. The target compounds were separated by

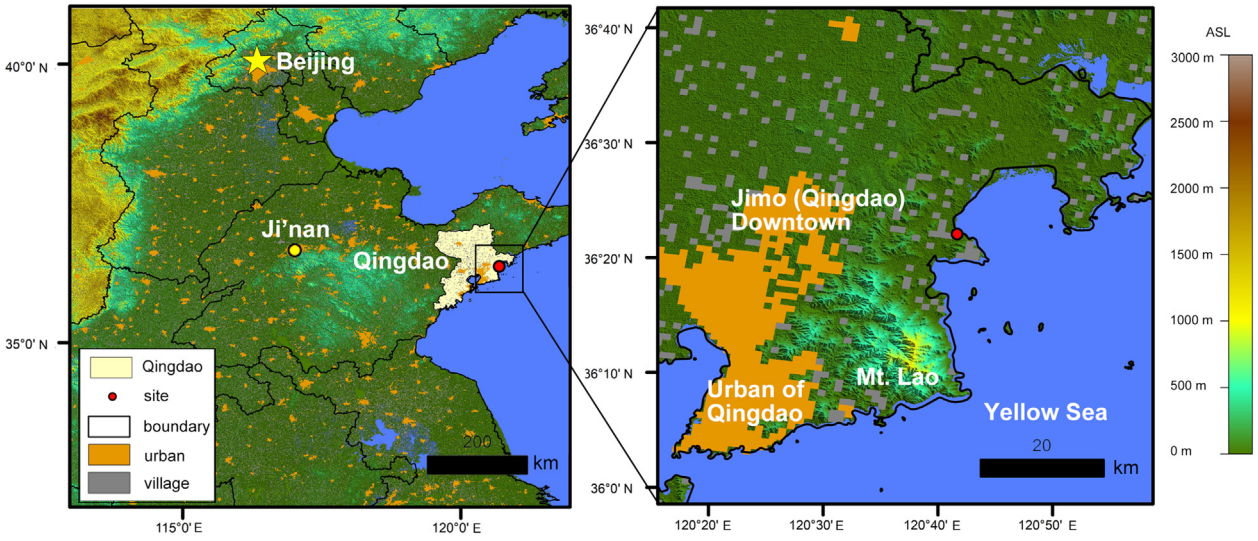

Fig. 1. Map showing the locations of Qingdao and the measurement site.

chromatographic column with the aid of Deans Switch technology and detected by flame ionization detector (FID) (C_2–C_3 compounds) and MS detector (C_4–C_{12} compounds). The single-point calibration and multi-point calibration were performed every five days and one month, respectively, using the standard gases of PAMS and TO15. The detection limits of the measured VOCs were in the range of 0.02 ppbv to 0.94 ppbv, and the measurement precision was about 5%.

O_3 was measured by a commercial UV photometric analyzer (*Model 49i, Thermo Scientific, USA*). CO was detected with a non-dispersive infrared analyzer (*Model 48i, Thermo Scientific, USA*). NO and NO_2 were observed with a chemiluminescence instrument (*Model 42i, Thermo Scientific, USA*). SO_2 was detected with a pulsed fluorescent gas analyzer (*Model 43i, Thermo Scientific, USA*). Their detection limits were 0.5 ppbv, 40 ppbv, 0.05 ppbv, and 0.12 ppbv, respectively. The meteorological parameters (wind speed, wind direction, relative humidity, and temperature) were obtained from an ambient air quality monitoring station of Qingdao, about 2 km away from the sampling site.

2.3. Observation-based box model

An observation-based box model was used to simulate the formation of PAN and evaluate its impact on O_3 production in this study. The chemical mechanism of this model was derived from the Regional Atmospheric Chemical Mechanism version 2 (RACM2), which has been successfully used to simulate O_3 formation and PAN budget (Fischer et al., 2014; Gross and Stockwell, 2003; Sun et al., 2020). The observation-based model contains 17 stable inorganic species, 4 short-lived inorganic species, 55 stable organic species, 43 short-lived organic species, and 363 chemical reactions. It should be noted that some secondary-generation precursors of PAN, such as acetaldehyde, MGLY, MACR, MVK, and glyoxal, were not measured in the present study, and their concentrations were simulated by the model with constraints of measured their first-generation hydrocarbon precursors. Physical processes such as dry deposition and dilution mixing were considered through the diurnal variations of boundary layer height. It was assumed that the PBL height increased from 300 m at dawn to 1500 m at 14:00 local time, then kept constant till the dust, and decreased to 300 m again afterward (Xue et al., 2014a). Photolysis frequencies were calculated within the model as a function of the solar zenith angle with an assumption of clear sky conditions. The dilution effect was considered by adopting a dilution mixing rate, which is a function of the variation of the PBL height. The emission rates of VOCs and NO_x were not included in the model. The measured species (e.g., PAN, O_3, NO_x, CO, SO_2, and VOCs) and meteorological parameters (temperature and relative humidity) were set as input with a 1-h time resolution to constrain the model. The model was pre-run for two days to reach the steady-state of unconstrained species. Note that a major shortcoming of the chemical box model is the lack of representation of atmospheric physical processes. Considering the relatively small surface winds, with average wind speeds of 1.5 m s^{-1} and 2.1 m s^{-1} in summer and autumn, the modelling analyses were conducted for all the measurement days except for those with precipitations. The model was constrained by the measured PAN concentrations to evaluate its impacts on the in-situ O_3 formation. It should be kept in mind that the observed PAN may come from both local production and, to a lesser extent, regional transport.

In this study, PAN formation has mainly been discussed through the production and loss of PA radical as commonly used in previous studies (Sun et al., 2020; Xue et al., 2014a). All reactions related to PA radical were tracked and grouped into several pathways. The production rates were calculated as the sum of reaction rates of PAN decomposition, a series of reactions involving acetaldehyde, acetone, methylglyoxal, methyl ethyl ketone, methyl vinyl ketone, methacrolein, other OVOCs, ozonolysis of isoprene, and reactions of O_3 with other VOCs. The PA loss rates were calculated as the sum of PA + NO_2, PA + NO and NO_3, PA + HO_2, and PA + RO_2 (a series of reactions). The calculations of O_3 production and loss rates were adopted from our previous studies (Chen et al., 2020; Xue et al., 2016).

The sensitivity of PAN and O_3 formation to its precursors was calculated using the relative incremental reactivity (RIR) simulated by the model. RIR_{PAN} and RIR_{O3} were defined as the ratios of the decrease in net PAN and O_3 production rates to the decrease in precursor concentrations (Chen et al., 2020; Xue et al., 2014a).

$$RIR_{PAN}(X) = \frac{\frac{P_{PAN}(X) - P_{PAN}(X-\Delta X)}{P_{PAN}}}{\Delta S(X)} \quad (1)$$

$$RIR_{O3}(X) = \frac{\frac{P_{O3}(X) - P_{O3}(X-\Delta X)}{P_{O3}}}{\Delta S(X)} \quad (2)$$

X represents a specific precursor (NO_x, a certain species/group of VOCs, and CO in this study); S(X) is the measured concentration of X; ΔX is the change in the mixing ratio of X due to a hypothetical change ΔS(X) (20% in this study). A positive RIR value indicates a promotion of the precursor in PAN or O_3 production, whereas a negative value indicates an inhibition. The larger value indicates a greater sensitivity of the production to the specific precursor.

A constrained scenario was designed to evaluate the impact of PAN on O_3 production via the radical pathway. In this scenario, both production and loss pathways of PAN were closed while other conditions, including NO_x concentrations, were the same as the base simulation. The differences between these two simulations, including O_3 production rates and RO_x radical concentrations, were used to estimate the impact of PAN on O_3 production. Another two simulations that increased or decreased NO_x by 20% were used to check the sensitivity of O_3 production to NO_x at this observation site.

3. Results and discussion

3.1. General description

Descriptive statistics of major trace gases and meteorological parameters in both autumn and summer are summarized in Table 1, and their temporal variations are provided in Fig. S1. As a typical coastal site, the station is significantly affected by both the Asian Monsoon and sea-land breezes. As shown from Fig. S2, the dominant surface winds at the study site were southeasterly and northwesterly during the summer and autumn campaigns, respectively. An exception in summer was the strong northwesterly winds observed during August 14–17, 2019, which was mainly due to the passage of Typhoon Lekima. The effect of sea-land breezes was also evidenced by the observed diurnal variations of surface winds with southerly winds during the daytime and northerly winds at night. The hourly averaged concentrations of NO, NO_2, CO, and SO_2 were 1.6 ± 4.2 ppbv, 16.7 ± 9.6 ppbv, 361 ± 187 ppbv, and 2.7 ± 1.2 ppbv, respectively, in autumn, which were higher (2.4, 3.3, 1.2, and 1.5 times, respectively) than those in summer. This is consistent with the shift of the dominant wind directions from the north in autumn to the south or eastern south in summer (Fig. S2); air masses from north China (continental air masses) usually contain higher pollutant concentrations, while south or eastern south air masses from the sea was relatively clean (Yang et al., 2021). Fig. S2b and S2d show that both southeasterly and northwesterly winds alternated at the study site in summer, both of which were associated with distinct pollution levels of PAN. This suggests the impact of sea-land breezes on the observed air quality as this coastal site. The mean concentration level of NO was only 0.7 ± 0.5 ppbv in summer, indicating that this sampling site was a relatively clean area in summer. However, occasionally high concentrations up to 6.0 ppbv of NO were observed, suggesting that polluted air masses could also affect this site. The concentration levels of the main VOCs measured are provided in Table 2. The levels of total VOCs in both seasons were relatively low (7.55 ± 4.34 ppbv in autumn and 5.99 ± 4.56 ppbv in summer) compared with previous measurements in urban or suburban areas in China (Sun et al., 2020; Zeng et al., 2019). Alkanes and Alkenes were the main VOC species, accounting for about 80% of total VOCs in both seasons. The levels of both isoprene and aromatics were low, mainly due to the low vegetation coverage and low anthropogenic emissions in this area. Similar to primary inorganic pollutants, the level of total VOCs was higher in autumn than in summer. In contrast, relatively higher PAN and O_3 levels were observed in summer ($P < 0.01$). The average concentrations of PAN and O_3 in summer were 0.81 ± 0.87 ppbv and 44.8 ± 20.8 ppbv, respectively, in comparison to their average concentrations of 0.75 ± 0.79 ppbv and 38.7 ± 20.6 ppbv in autumn.

Table 1
Descriptive statistics of hourly concentrations of PAN and related species and meteorological parameters at coastal Qingdao in autumn and summer campaigns.

Species	Autumn			Summer		
	Mean (SD)	Median	Max	Mean (SD)	Median	Max
PAN (ppbv)	0.75 (0.79)	0.56	5.83	0.81 (0.87)	0.53	7.82
O_3 (ppbv)	38.7 (20.6)	35.0	110.1	44.8 (20.8)	42.7	113.5
NO (ppbv)	1.6 (4.2)	0.28	55.6	0.7 (0.5)	0.5	6.0
NO_2 (ppbv)	16.7 (9.6)	13.0	56.1	4.8 (4.4)	3.1	30.8
CO (ppbv)	361 (187)	300	1416	289 (200)	266	1110
SO_2 (ppbv)	2.7 (1.2)	2.3	12.1	1.8 (0.9)	1.5	12.1
Temp (°C)	14.0 (5.2)	13.5	26.9	27.4 (2.9)	27.0	36.3
RH (%)	68 (21)	68	100	80 (11)	82	99

Figs. 2 and S3 show the average diurnal variations of major trace gases and VOCs, respectively. Their diurnal variations in autumn were similar to those measured in the continental areas, usually with a significant peak in the morning rush hour and more prominent concentration variations (Sun et al., 2020; Zeng et al., 2019). This was particularly true for NO, with a peak concentration exceeding 5 ppbv in the morning and about 5 times higher than that in summer. Both the production and removal rates of O_3 were faster in autumn, forming a sharper peak compared with that in summer. The PAN levels peaked 2 h earlier in summer (11:00 LT) than that in autumn (13:00 LT), while its peak concentration was higher in summer (1.18 ppbv versus 1.02 ppbv). The earlier but higher peak of PAN in summer should be caused by the higher intensive solar radiation and temperatures, which promoted both the production and decomposition rates of PAN (Qiu et al., 2019; Xue et al., 2014a; Zhang et al., 2009). A detailed discussion about PAN formation is provided in Section 3.2.

As both produced from the photochemical reactions of VOCs and NO_x, PAN and O_3 generally show a relatively close relationship. The daily maximum PAN to O_3 ratio was usually applied to indicate their relative photochemical production efficiencies (Roberts et al., 1995). Fig. 3 shows positive correlations ($R^2 = 0.51$ and 0.54, respectively) between daily maximum values of PAN and O_3 in autumn and summer, and the regression slopes are 0.043 and 0.055 (ppbv/ppbv), respectively. These indicated that 4.3 and 5.5 PAN molecules were produced for 100 O_3 molecules formed in autumn and summer, respectively. Tables S1 and S2 summarize the simultaneous measured PAN and O_3 concentrations and the daily maximum PAN to O_3 ratio measured in other areas of China. On average, the mean levels of PAN and O_3 in this study were lower than those measured in the polluted urban areas, while the maximum PAN concentrations (5.83 ppbv in autumn and 7.82 ppbv in summer in this study) were comparable to that measured in most polluted cities (3.10–13.47 ppbv). The daily maximum PAN to O_3 ratio was also comparable to or even higher (0.027–0.1) than that measured in urban or suburban areas. According to concentration versus wind speed/direction plots provided in Fig. S2c and Fig. S2d, high PAN concentrations in autumn showed no relationship with wind directions. In contrast, the high concentrations in summer mainly occurred in the northwesterly wind direction, usually containing higher PAN precursor concentrations. This indicated that although this site was a relatively clean coastal area, severe photochemical pollution and efficient PAN formation might also occur, especially in summer.

3.2. Formation mechanism of PAN

3.2.1. Formation and fate of PA radical

Fig. 4a and b shows the modeled formation and loss rates of PA radical in autumn and summer, respectively. An important feature was that the total production rate of PA radical was higher in summer than in autumn, 3.45 ppbv h^{-1} versus 1.07 ppbv h^{-1} ($P < 0.01$). This was mainly due to the higher PAN decomposition rate in summer, with a daytime average of 2.36 ppbv h^{-1} in summer versus 0.61 ppbv h^{-1} in autumn. Other formation sources such as reactions of acetaldehyde and methylglyoxal also became higher in summer ($P < 0.01$), e.g., 0.85 ppbv h^{-1} from acetaldehyde in summer versus 0.37 ppbv h^{-1} in autumn. The peak time of the production rates was similar to the diurnal variation of PAN, peaked at 11:00 LT in summer and about at noon in autumn. These results further indicated that there was efficient PAN production in summer at this site.

On average, PAN decomposition was the most significant proportion of the daytime PA radical source, accounting for 57% and 68% in autumn and summer, respectively. Other significant sources were reactions of acetaldehyde (35% and 25%, respectively) and methylglyoxal (6% and

Table 2
Descriptive statistics of the measured VOCs at coastal Qingdao in autumn and summer campaigns (unit: ppbv).

Species	Autumn			Summer		
	Mean (SD)	Median	Max	Mean (SD)	Median	Max
Ethane	1.74 (0.54)	1.61	5.09	0.96 (0.71)	0.73	3.73
Propane	1.26 (0.94)	0.96	5.84	1.50 (1.57)	0.92	8.60
n-Butane	0.49 (0.45)	0.33	2.82	0.50 (0.58)	0.26	3.74
Isobutane	0.45 (0.28)	0.35	1.52	0.25 (0.16)	0.22	1.31
Cyclopentane	0.03 (0.03)	0.02	0.26	0.02 (0.03)	0.01	0.52
n-Pentane	0.05 (0.05)	0.03	0.39	0.03 (0.02)	0.03	0.14
Isopentane	0.20 (0.21)	0.13	1.55	0.13 (0.15)	0.07	1.31
Cyclohexane	0.03 (0.04)	0.01	0.33	0.01 (0.00)	0.01	0.04
2,2-Dimethylbutane	0.01 (0.01)	0.01	0.05	0.01 (0.00)	0.01	0.02
2,3-Dimethylbutane	0.10 (0.11)	0.07	0.67	0.06 (0.05)	0.05	0.36
Methylcyclopentane	0.04 (0.07)	0.02	0.89	0.01 (0.01)	0.01	0.10
2-Methylpentane	0.10 (0.11)	0.07	0.80	0.09 (0.06)	0.07	0.40
3-Methylpentane	0.06 (0.10)	0.03	1.00	0.02 (0.02)	0.02	0.18
2,3-Dimethylpentane	0.08 (0.07)	0.05	0.43	0.01 (0.01)	0.01	0.06
2,4-Dimethylpentane	0.01 (0.01)	0.01	0.06	0.01 (0.00)	0.01	0.03
2-Methylhexane	0.02 (0.01)	0.02	0.09	0.01 (0.01)	0.01	0.09
3-Methylhexane	0.02 (0.01)	0.01	0.11	0.01 (0.00)	0.01	0.03
n-Heptane	0.02 (0.02)	0.01	0.17	0.01 (0.01)	0.01	0.08
n-Dodecane	0.03 (0.04)	0.01	0.30	0.03 (0.02)	0.02	0.21
Ethylene	0.77 (0.61)	0.60	5.03	0.29 (0.35)	0.18	3.58
Propylene	0.20 (0.16)	0.16	1.26	0.20 (0.14)	0.17	1.34
Butadiene	0.05 (0.13)	0.03	1.90	0.03 (0.02)	0.02	0.17
1-Butene	0.29 (0.28)	0.24	1.36	0.29 (0.26)	0.19	1.56
Trans-2-butene	0.02 (0.02)	0.01	0.17	0.01 (0.01)	0.01	0.07
Cis-2-butene	0.10 (0.04)	0.10	0.32	0.08 (0.03)	0.07	0.17
Isoprene	0.01 (0.01)	0.01	0.04	0.04 (0.04)	0.03	0.24
1-Pentene	0.08 (0.07)	0.06	0.59	0.07 (0.05)	0.06	0.42
Trans-2-pentene	0.05 (0.05)	0.03	0.29	0.02 (0.02)	0.02	0.11
1-Hexene	0.01 (0.02)	0.01	0.19	0.05 (0.18)	0.03	3.90
Acetylene	0.24 (0.14)	0.22	1.26	0.15 (0.13)	0.10	0.83
Benzene	0.13 (0.16)	0.07	1.11	0.05 (0.05)	0.04	0.40
Toluene	0.10 (0.16)	0.04	1.06	0.04 (0.05)	0.02	0.55
Ethylbenzene	0.05 (0.08)	0.02	0.53	0.02 (0.03)	0.01	0.23
M/p-Xylene	0.02 (0.01)	0.01	0.11	0.01 (0.00)	0.01	0.03
o-Xylene	0.02 (0.01)	0.01	0.07	0.01 (0.00)	0.01	0.01
4-Ethyltoluene	0.09 (0.17)	0.02	1.31	0.03 (0.05)	0.01	0.45
2-Ethyltoluene	0.06 (0.10)	0.02	0.57	0.03 (0.04)	0.01	0.31
1,2,4-Trimethylbenzene	0.04 (0.04)	0.02	0.19	0.01 (0.01)	0.01	0.07
1,3,5-Trimethylbenzene	0.02 (0.02)	0.02	0.13	0.01 (0.01)	0.01	0.05
1,4-Diethylbenzene	0.02 (0.02)	0.01	0.13	0.01 (0.00)	0.01	0.02
Acrolein	0.07 (0.05)	0.07	0.25	0.02 (0.01)	0.02	0.08
Acetone	0.58 (0.41)	0.61	2.69	0.93 (0.51)	0.88	3.20
Methyl ethyl ketone	0.07 (0.06)	0.05	0.45	0.06 (0.05)	0.04	0.41
Methyl methacrylate	0.03 (0.03)	0.03	0.31	0.01 (0.01)	0.01	0.17
Ethylacetate	0.12 (0.13)	0.07	1.20	0.08 (0.07)	0.06	0.53
Total	7.55 (4.34)	6.10	25.84	5.99 (4.56)	4.02	27.78

9%, respectively). Without considering the transformation between PAN and PA, sources from acetaldehyde reactions would be 80% and 78% in autumn and summer, respectively, and sources from methylglyoxal would be 13% and 16%, respectively. Other pathways were relatively minor. These quantified sources were similar to other previous studies in China (Liu et al., 2018; Xue et al., 2014a; Zeng et al., 2019; Zhang et al., 2019a). It should be noted that acetaldehyde and methylglyoxal had either primary or secondary sources (Qian et al., 2019). Thus, it is necessary to identify the key first-generation precursors of PAN to better control the photochemical pollution, which will be discussed in the following section.

For the fate of PA radical, the reaction with NO_2 forming PAN accounted for 62% and 66% of their total loss rates in autumn and summer, respectively. However, a large proportion of it would react with NO (both were 29% in autumn and summer), forming a series of products, e.g., CH_3O_2, HO_2, and HCHO, thus potentially affecting the radical cycling and oxidation capacity of the atmosphere. Other fates of PA radical were reacting with RO_2 and HO_2 radicals, accounting for about 9% and 5% in autumn and summer, respectively. PA radical is one of the most abundant organic peroxy radicals in the troposphere, accounting for 7% and 9% of the modeled total RO_2 concentrations in autumn and summer, respectively, in this study. Thus, PAN photochemistry would undoubtedly affect radical cycling and subsequent O_3 production at this observation site.

3.2.2. Sensitivity of PAN and O_3 to precursors

To identify the critical first-generation precursors of PAN and O_3 and compare their sensitivity differences, we performed the RIR analysis based on the model simulations. Fig. 5a and b shows the model-calculated RIR of PAN and O_3 for different species/groups, including CO, NO_x, isoprene, alkanes, alkenes, and aromatics in autumn and summer, respectively.

For O_3, the RIR_{O3} values for NO_x and VOCs were positive in both autumn and summer, indicating that O_3 production was in the transition regime in this area and limited by both NO_x and VOCs. This result was similar to those obtained in the rural areas (Wang et al., 2017; Zong et al., 2018) but in contrast to the results from polluted urban areas of China, where O_3 production was usually in the VOC-limited regime (Xue et al., 2016, 2014b). Alkenes showed the largest RIR values among the measured VOC groups in both autumn and summer, with a midday average of 0.40 and 0.26, respectively. The RIR values of isoprene, alkanes, and aromatics were relatively small due to their low

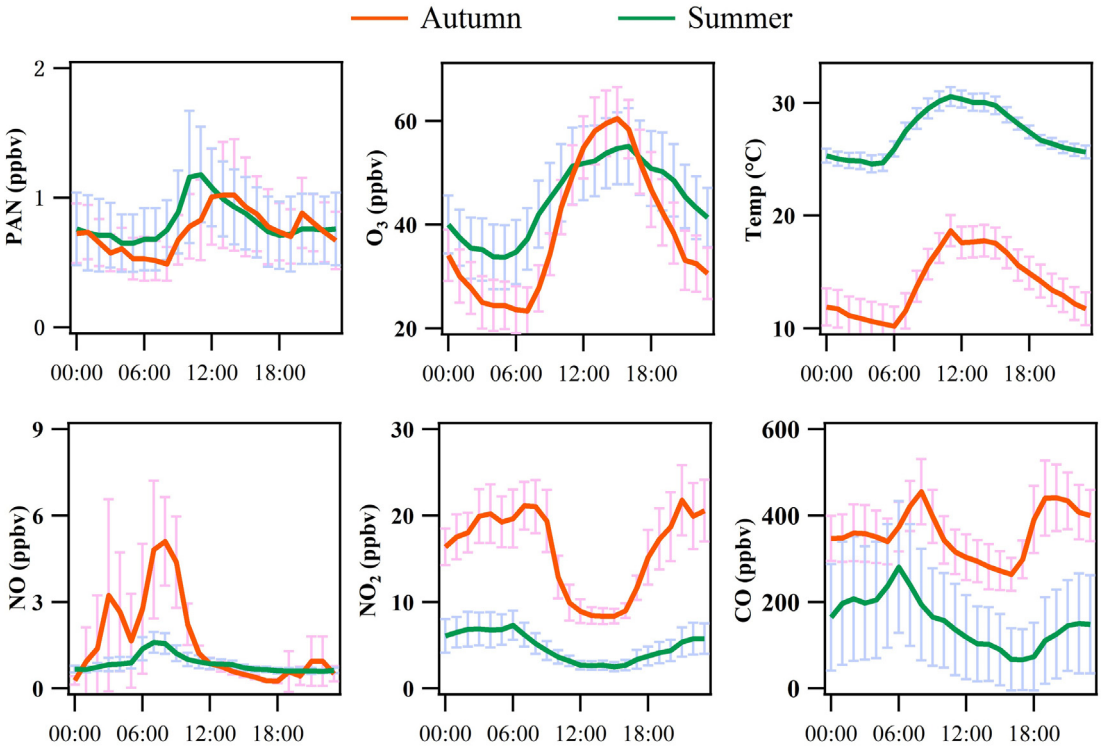

Fig. 2. Diurnal variations of PAN and related species in autumn (brown line) and summer (green line) in the coastal atmosphere of Qingdao. The error bar indicates one-third of the standard deviation. (For interpretation of the references to colour in this figure legend, the reader is referred to the web version of this article.)

concentrations or low reactivities. The comparison of the RIR values of NO_x and alkenes showed that alkenes were greater in autumn (0.40 versus 0.26 for alkenes), while NO_x was greater in summer (0.28 versus 0.13). This was consistent with the higher NO_x concentrations in autumn and suggested that the control of NO_x in summer and VOCs in autumn should be more effective for regulating O_3 pollution in this area.

For PAN, its production was mainly controlled by NO_x and alkenes in both summer and autumn. However, the RIR_{PAN} values for VOCs and NO_x were higher in autumn than in summer, especially for alkenes

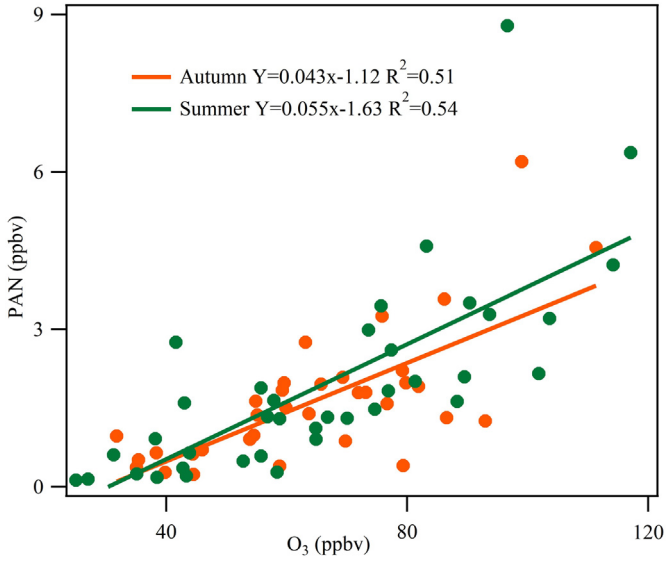

Fig. 3. Correlations between daily maximum PAN and daily maximum O_3 in autumn (brown) and summer (green). (For interpretation of the references to colour in this figure legend, the reader is referred to the web version of this article.)

(0.88 versus 0.15). The property of rapidly thermal decomposition of PAN at high temperatures may be the main reason. In summer, the primary source of PA radical was from PAN decomposition (accounting for 68%), and the source from the oxidation of VOCs was smaller than that in autumn. Therefore, the sensitivity of PAN production to VOCs became lower in summer. The NO_x concentration in summer was significantly lower than that in autumn; thus, the sensitivity of PAN should be greater in summer. However, the rapid PAN decomposition may accelerate the recycling of NO_2, and the reduction of NO_x (20%) significantly increased PA radical concentration (13%) in summer. This may make up for the lack of NO_x, thus reducing its sensitivity to NO_x.

When comparing RIR_{PAN} and RIR_{O3}, RIR_{PAN} for VOCs and NO_x were higher than the corresponding RIR_{O3} values in autumn ($P < 0.01$), suggesting that the overall PAN formation tended to be more sensitive to these precursors compared with O_3. The RIR_{PAN} for alkenes was up to 0.88 in autumn, much higher than RIR_{O3} for alkenes (0.40) and RIR_{PAN} for NO_x (0.30). This was because only a small proportion of the VOCs that could produce PA radical could form PAN; therefore, compared with the VOCs that produced O_3, the VOCs that produced PAN were more insufficient than NO_x (Fischer et al., 2014). RIR_{PAN} for both VOCs and NO_x were lower than RIR_{O3} in summer; this might also be due to the rapid decomposition of PAN. It should be noted that the effect of NO_x on PAN and O_3 production was very variable from day-to-day. Fig. 6 presents the correlation between RIR_{PAN} and RIR_{O3} for NO_x in day-to-day calculations. The consistent variations implied the similar formation process of PAN and O_3, while RIR_{PAN} values for NO_x were negative in quite a few days in summer. This suggested that NO_x suppressed the production of PAN under some conditions of the summer. In the case of 20% NO_x reduction, the modeled PA radical concentration increased 13% mainly due to the reduced consumption from the reaction of NO+PA, while RO_2 radical increased only 3%, partially offset by the reduced OH radicals. This indicated that under high-temperature conditions, the dominant influence path of NO_x on PAN and O_3 production might be significantly different.

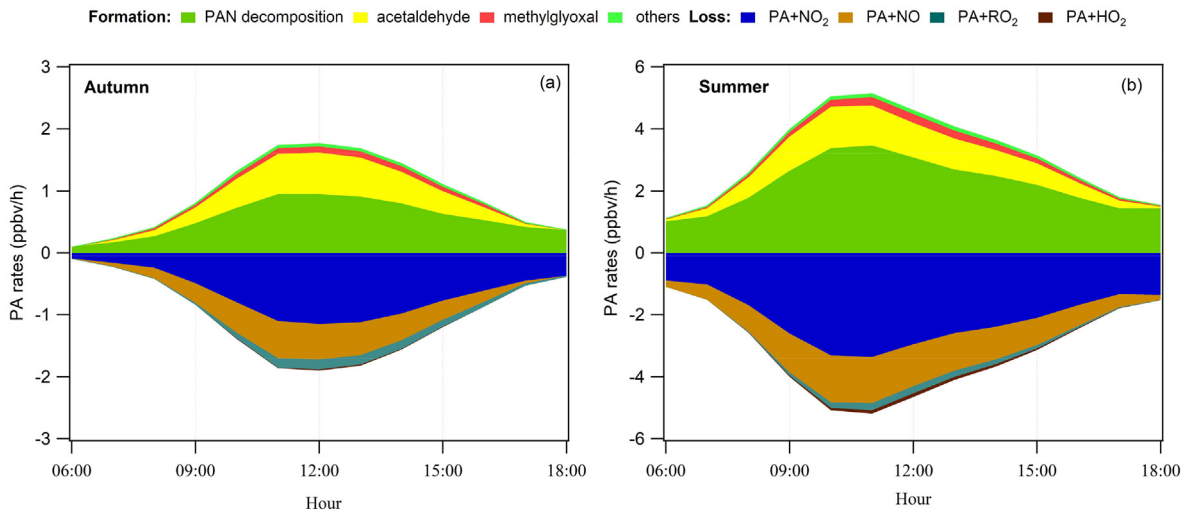

Fig. 4. Modeled average formation and loss rates of PA radical in coastal Qingdao in autumn (a) and summer (b).

3.3. Impacts of PAN on O_3 production

PAN photochemistry could affect the cycle of atmospheric radicals, and thus inevitably regulating O_3 production. In this section, we discuss the impact of PAN on O_3 production and pay attention to the influence via the radical pathway. We focused on the summer campaign as it was affected by both clean marine air masses and polluted continental air masses. Fig. S4 shows the relative change of net O_3 production rates (net $P(O_3)$) in the base scenario to that simulated without PAN photochemistry. A positive value of Δnet $P(O_3)$ indicated that the PAN photochemistry promoted O_3 production, while the negative values indicated that PAN inhibited O_3 production. Both promotion and inhibition effects of PAN on O_3 production were observed in summer. On average, out of the simulated 34 days, 18 days shows a "promotion effect", and 16 days are identified with an "inhibition effect".

Fig. 7 shows the corresponding change of modeled net $P(O_3)$ and RO_x radicals. The detailed variations of O_3 production and destruction pathways are provided in Fig. S5, and the measured species and parameters in "promotion effect" days and "inhibition effect" days are summarized in Table S3. On the "promotion effect" days, the net $P(O_3)$ decreased from 9.8 ± 2.1 ppbv h^{-1} to 8.0 ± 1.5 ppbv h^{-1} without considering the PAN photochemistry, while during the "inhibition effect" days, the net $P(O_3)$ increased from 6.1 ± 1.2 ppbv h^{-1} to 6.6 ± 1.2 ppbv h^{-1}. In terms of percentage, PAN photochemistry accounted for 18% and 8% of the net $P(O_3)$ on the "promotion effect" days and "inhibition effect" days, respectively. This change could be well explained by the corresponding concentration change of modeled RO_x radicals. On the "promotion effect" days, the daytime averaged concentrations of OH and RO_2 decreased from 1.7×10^7 molecules cm^{-3} and 5.4×10^8 molecules cm^{-3} to 1.2×10^7 molecules cm^{-3} and 4.2×10^8 molecules cm^{-3}, while HO_2 increased from 6.0×10^8 molecules cm^{-3} to 6.5×10^8 molecules cm^{-3}. The significant concentration decrease (22%) of RO_2 without PAN photochemistry was the main reason for the $P(O_3)$ decrease. However, on the "inhibition effect" days, despite a small decrease of RO_2 from 3.4×10^8 molecules cm^{-3} to 3.3×10^8 molecules cm^{-3}, the concentrations of OH and HO_2 increased from 1.3×10^7 molecules cm^{-3} and 3.8×10^8 molecules cm^{-3} to 1.4×10^7 molecules cm^{-3} and 4.2×10^8 molecules cm^{-3}. The concentration increase of HO_2 (9%) leaded to an increase of net $P(O_3)$ without PAN photochemistry during the "inhibition effect" days.

PAN could be the reservoir of PA radical, acting as its temporary sink or source depending on the environmental conditions. In the simulations of this study, the concentration of NO_x was constrained in the model; thus, the impact of PAN on O_3 production was mainly realized

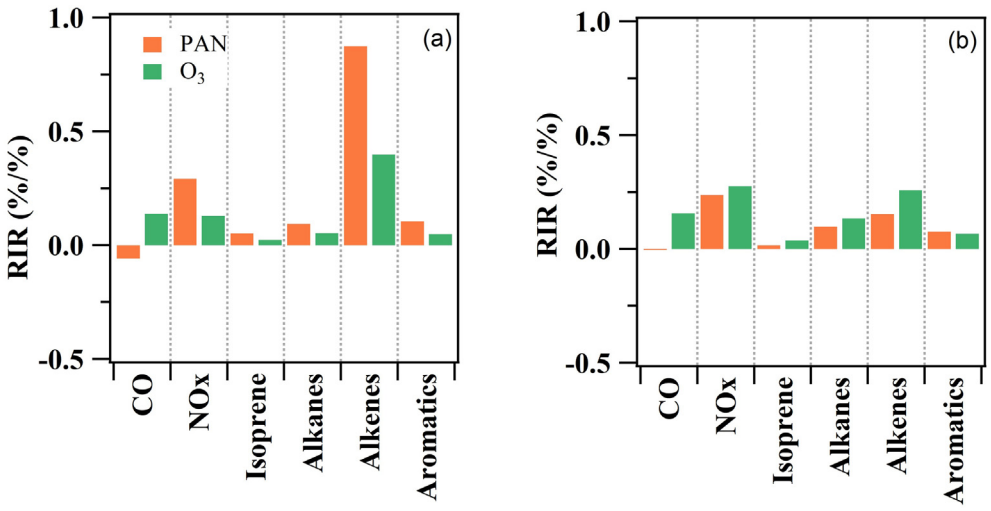

Fig. 5. Model-calculated midday (09:00–15:00 LT) averaged RIR values of PAN and O_3 for various precursor species/groups in autumn (a) and summer (b).

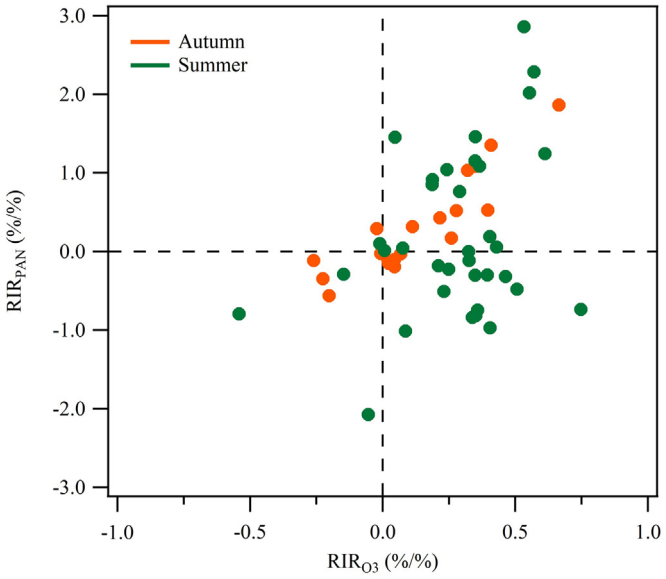

Fig. 6. Correlation between model-calculated RIR_{PAN} and RIR_{O3} for NO_x in autumn (brown) and summer (green). (For interpretation of the references to colour in this figure legend, the reader is referred to the web version of this article.)

by affecting the cycling of the radicals. The temperature and RH were comparable between the "promotion effect" days and "inhibition effect" days, while wind speeds were much lower on "promotion effect" days than that of "inhibition effect" days (Fig. S6), facilitating the accumulation of air pollutions, while the mixing ratios of the air pollutants (except for NO) were much higher. Generally, PAN tended to suppress the in-situ O_3 production by competing with O_3 precursors and terminating radical chain reactions under the low-NO_x and low-RO_x circumstances but could enhance the O_3 production by providing more RO_2 radicals and increasing the atmospheric oxidation capacity with the presence of sufficient NO_x. We compared the impact of PAN on O_3 production via the radical pathway to that of a 20% increase or decrease of NO_x. The daytime averaged net $P(O_3)$ only increased from 8.1 ± 2.5 ppbv h^{-1} to 8.2 ± 2.6 ppbv h^{-1} or decreased to 7.8 ± 2.5 ppbv h^{-1} with a 20% decrease or increase of NO_x. The results obtained in this study confirmed that PAN could affect O_3 production via radical cycling, but the impact was highly dependent on the environmental conditions.

4. Conclusions

In this study, PAN and O_3 were simultaneously measured in a coastal area of Qingdao in autumn 2018 and summer 2019. With the aid of an observation-based box model, the formation of PAN and its sensitivities to precursors and differences from O_3 formation were explored. Acetaldehyde and methylglyoxal were the main contributors of VOCs to PAN formation, and the photochemical formation of PAN was controlled by both NO_x and VOCs in this coastal area.

The formation of PAN and O_3 showed similar sensitivities to their precursors, but RIR_{PAN} for both NO_x and VOCs were larger than RIR_{O3} in autumn while smaller in summer. The seasonal variations of RIR_{PAN} were mainly caused by the property of rapid decomposition of PAN at high temperatures in summer. In terms of day-to-day calculations, NO_x suppressed PAN formation on quite a few days in summer via the consumption of PA radicals while still promoted O_3 production these

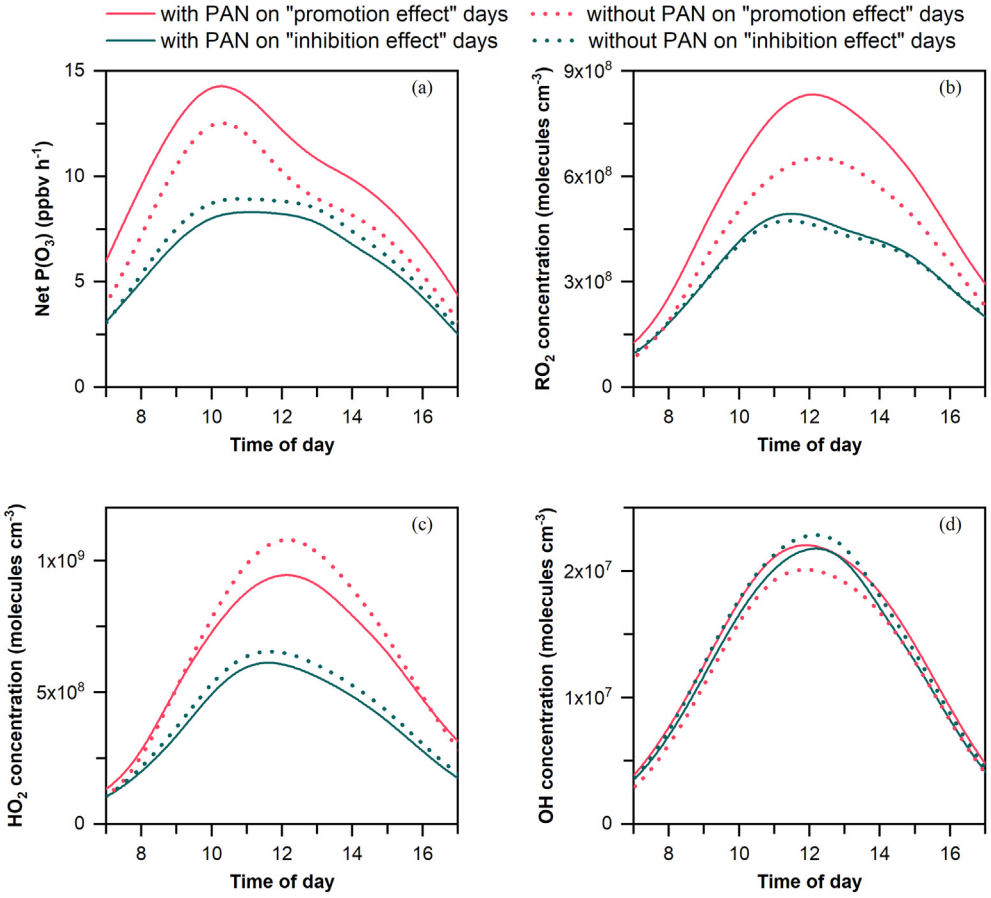

Fig. 7. Model-simulated (a) net O_3 production rate, (b) RO_2, (c) HO_2, and (d) OH with (solid line) or without (dotted line) PAN photochemistry on the "promotion effect" days (red) and "inhibition effect" days (green). (For interpretation of the references to colour in this figure legend, the reader is referred to the web version of this article.)

days. The dominant influence path of NO_x on PAN and O_3 production might be significantly different under high-temperature conditions.

The impact of PAN chemistry on O_3 production was explored through the zero-out sensitivity simulations. Both promotion and inhibition effects of PAN on O_3 production were confirmed. During the "promotion effect" days ("inhibition effect" days), daytime averaged net O_3 production rates decreased by 18% (increased by 8%) without considering PAN photochemistry. This was mainly caused by the significant increase of RO_2 radicals on the "promotion effect" days and a slight decrease of HO_2 radicals on the "inhibition effect" days affected by PAN photochemistry via the radical cycling pathway. The impact of PAN on O_3 production should be explored in more environmental conditions, and be paid particular attention to the effect of PAN on atmospheric oxidation capacity.

CRediT authorship contribution statement

Yuhong Liu: Conceptualization, Formal analysis, Writing – original draft. **Hengqing Shen:** Conceptualization, Formal analysis, Writing – original draft. **Jiangshan Mu:** Investigation, Data curation. **Hongyong Li:** Investigation, Data curation. **Tianshu Chen:** Investigation, Data curation. **Juan Yang:** Data curation. **Ying Jiang:** Data curation. **Yujiao Zhu:** Data curation, Resources. **He Meng:** Data curation, Resources. **Can Dong:** Funding acquisition, Resources. **Wenxing Wang:** Supervision, Resources. **Likun Xue:** Conceptualization, Funding acquisition, Project administration, Writing – review & editing.

Declaration of competing interest

The authors declare that they have no known competing financial interests or personal relationships that could have appeared to influence the work reported in this paper.

Acknowledgments

This work was funded by Shandong Provincial Science Foundation for Distinguished Young Scholars (ZR2019JQ09), the National Natural Science Foundation of China (41922051 and 41905113), and the Jiangsu Collaborative Innovation Center for Climate Change.

Appendix A. Supplementary data

Supplementary data to this article can be found online at https://doi.org/10.1016/j.scitotenv.2021.146265.

References

Aikin, A.C., Herman, J.R., Maier, E.J., McQuillan, C.J., 1982. Atmospheric chemistry of ethane and ethylene. J. Geophys. Res. Oceans 87, 3105–3118.
Atkinson, R., Baulch, D.L., Cox, R.A., Crowley, J.N., Hampson, R.F., Hynes, R.G., et al., 2006. Evaluated kinetic and photochemical data for atmospheric chemistry: volume II - gas phase reactions of organic species. Atmos. Chem. Phys. 6, 3625–4055.
Chen, T., Xue, L., Zheng, P., Zhang, Y., Liu, Y., Sun, J., et al., 2020. Volatile organic compounds and ozone air pollution in an oil production region in northern China. Atmos. Chem. Phys. 20, 7069–7086.
Crowley, J.N., Pouvesle, N., Phillips, G.J., Axinte, R., Fischer, H., Petaja, T., et al., 2018. Insights into HOx and ROx chemistry in the boreal forest via measurement of peroxyacetic acid, peroxyacetic nitric anhydride (PAN) and hydrogen peroxide. Atmos. Chem. Phys. 18, 13457–13479.
Fischer, E.V., Jaffe, D.A., Reidmiller, D.R., Jaegle, L., 2010. Meteorological controls on observed peroxyacetyl nitrate at Mount Bachelor during the spring of 2008. J. Geophys. Res.-Atmos. 115, 18.
Fischer, E.V., Jacob, D.J., Yantosca, R.M., Sulprizio, M.P., Millet, D.B., Mao, J., et al., 2014. Atmospheric peroxyacetyl nitrate (PAN): a global budget and source attribution. Atmos. Chem. Phys. 14, 2679–2698.
Gross, A., Stockwell, W.R., 2003. Comparison of the EMEP, RADM2 and RACM mechanisms. J. Atmos. Chem. 44, 151–170.
Jiang, Z., Worden, J.R., Payne, V.H., Zhu, L.Y., Fischer, E., Walker, T., et al., 2016. Ozone export from East Asia: the role of PAN. J. Geophys. Res.-Atmos. 121, 6555–6563.
LaFranchi, B.W., Wolfe, G.M., Thornton, J.A., Harrold, S.A., Browne, E.C., Min, K.E., et al., 2009. Closing the peroxy acetyl nitrate budget: observations of acyl peroxy nitrates (PAN, PPN, and MPAN) during BEARPEX 2007. Atmos. Chem. Phys. 9, 7623–7641.
Lee, G., Jang, Y., Lee, H., Han, J.-S., Kim, K.-R., Lee, M., 2008. Characteristic behavior of peroxyacetyl nitrate (PAN) in Seoul megacity, Korea. Chemosphere 73, 619–628.
Liu, L., Wang, X.F., Chen, J.M., Xue, L.K., Wang, W.X., Wen, L., et al., 2018. Understanding unusually high levels of peroxyacetyl nitrate (PAN) in winter in Urban Jinan, China. J. Environ. Sci. 71, 249–260.
Lonneman, W.A., Bufalini, J.J., Seila, R.L., 1976. PAN and oxidant measurement in ambient atmospheres. Environ. Sci. Technol. 10, 374–380.
Mills, G.P., Sturges, W.T., Salmon, R.A., Bauguitte, S.J.B., Read, K.A., Bandy, B.J., 2007. Seasonal variation of peroxyacetylnitrate (PAN) in coastal Antarctica measured with a new instrument for the detection of sub-part per trillion mixing ratios of PAN. Atmos. Chem. Phys. 7, 4589–4599.
Penkett, S.A., Brice, K.A., 1986. The spring maximum in Photooxidants in the northern-hemisphere troposphere. Nature 319, 655–657.
Qian, X., Shen, H., Chen, Z., 2019. Characterizing summer and winter carbonyl compounds in Beijing atmosphere. Atmos. Environ. 214, 116845.
Qiu, Y.L., Lin, W.L., Li, K., Chen, L., Yao, Q., Tang, Y.X., et al., 2019. Vertical characteristics of peroxyacetyl nitrate (PAN) from a 250-m tower in northern China during September 2018. Atmos. Environ. 213, 55–63.
Roberts, J.M., Tanner, R.L., Newman, L., Bowersox, V.C., Bottenheim, J.W., Anlauf, K.G., et al., 1995. Relationships between PAN and ozone at sites in eastern North America. J. Geophys. Res.-Atmos. 100, 22821–22830.
Singh, H.B., Hanst, P.L., 1981. Peroxyacetyl nitrate (PAN) in the unpolluted atmosphere - an important reservoir for nitrogen-oxides. Geophys. Res. Lett. 8, 941–944.
Stephens, E.R., 1969. In: Pitts Jr., J.N., Metcalf, R.L. (Eds.), The Formation, Reactions, and Properties of Peroxyacyl Nitrates (PANs) in Photochemical Air Pollution. Wiley-Interscience, New York, NY.
Stephens, E.R., Hanst, P.L., Doerr, R.C., Scott, W.E., 1956. Reactions of nitrogen dioxide and organic compounds in air. Ind. Eng. Chem. 48, 1498–1504.
Sun, M., Cui, J.N., Zhao, X.M., Zhang, J.B., 2020. Impacts of precursors on peroxyacetyl nitrate (PAN) and relative formation of PAN to ozone in a southwestern megacity of China. Atmos. Environ. 231, 11.
Temple, P.J., Taylor, O.C., 1983. World-wide ambient measurements of peroxyacetyl nitrate (PAN) and implications for plant injury. Atmos. Environ. 17, 1583–1587.
Tyndall, G.S., Cox, R.A., Granier, C., Lesclaux, R., Moortgat, G.K., Pilling, M.J., et al., 2001. Atmospheric chemistry of small organic peroxy radicals. J. Geophys. Res.-Atmos. 106, 12157–12182.
Wang, T., Xue, L.K., Brimblecombe, P., Lam, Y.F., Li, L., Zhang, L., 2017. Ozone pollution in China: a review of concentrations, meteorological influences, chemical precursors, and effects. Sci. Total Environ. 575, 1582–1596.
Wolfe, G.M., Cantrell, C., Kim, S., Mauldin, R.L., Karl, T., Harley, P., et al., 2014. Missing peroxy radical sources within a summertime ponderosa pine forest. Atmos. Chem. Phys. 14, 4715–4732.
Xue, L., Wang, T., Wang, X., Blake, D.R., Gao, J., Nie, W., et al., 2014a. On the use of an explicit chemical mechanism to dissect peroxy acetyl nitrate formation. Environ. Pollut. 195, 39–47.
Xue, L.K., Wang, T., Gao, J., Ding, A.J., Zhou, X.H., Blake, D.R., et al., 2014b. Ground-level ozone in four Chinese cities: precursors, regional transport and heterogeneous processes. Atmos. Chem. Phys. 14, 13175–13188.
Xue, L., Gu, R., Wang, T., Wang, X., Saunders, S., Blake, D., et al., 2016. Oxidative capacity and radical chemistry in the polluted atmosphere of Hong Kong and Pearl River Delta region: analysis of a severe photochemical smog episode. Atmos. Chem. Phys. 16, 9891–9903.
Yang, J., Shen, H., Guo, M.-Z., Zhao, M., Jiang, Y., Chen, T., et al., 2021. Strong marine-derived nitrous acid (HONO) production observed in the coastal atmosphere of northern China. Atmos. Environ. 244, 117948.
Zeng, L.W., Fan, G.J., Lyu, X.P., Guo, H., Wang, J.L., Yao, D.W., 2019. Atmospheric fate of peroxyacetyl nitrate in suburban Hong Kong and its impact on local ozone pollution. Environ. Pollut. 252, 1910–1919.
Zhang, J.M., Wang, T., Ding, A.J., Zhou, X.H., Xue, L.K., Poon, C.N., et al., 2009. Continuous measurement of peroxyacetyl nitrate (PAN) in suburban and remote areas of western China. Atmos. Environ. 43, 228–237.
Zhang, X., Chen, Z.M., He, S.Z., Hua, W., Zhao, Y., Li, J.L., 2010. Peroxyacetic acid in urban and rural atmosphere: concentration, feedback on PAN-NO_x cycle and implication on radical chemistry. Atmos. Chem. Phys. 10, 737–748.
Zhang, G., Mu, Y.J., Liu, J.F., Mellouki, A., 2012. Direct and simultaneous determination of trace-level carbon tetrachloride, peroxyacetyl nitrate, and peroxypropionyl nitrate using gas chromatography-electron capture detection. J. Chromatogr. A 1266, 110–115.
Zhang, H., Xu, X., Lin, W., Wang, Y., 2014. Wintertime peroxyacetyl nitrate (PAN) in the megacity Beijing: role of photochemical and meteorological processes. J. Environ. Sci. 26, 83–96.
Zhang, G., Mu, Y.J., Zhou, L.X., Zhang, C.L., Zhang, Y.Y., Liu, J.F., et al., 2015. Summertime distributions of peroxyacetyl nitrate (PAN) and peroxypropionyl nitrate (PPN) in Beijing: understanding the sources and major sink of PAN. Atmos. Environ. 103, 289–296.
Zhang, B.Y., Zhao, B., Zuo, P., Huang, Z., Zhang, J.B., 2019a. Influencing factors and prediction of ambient Peroxyacetyl nitrate concentration in Beijing, China. J. Environ. Sci. 77, 189–197.
Zhang, B.Y., Zhao, X.M., Zhang, J.B., 2019b. Characteristics of peroxyacetyl nitrate pollution during a 2015 winter haze episode in Beijing. Environ. Pollut. 244, 379–387.
Zong, R., Yang, X., Wen, L., Xu, C., Zhu, Y., Chen, T., et al., 2018. Strong ozone production at a rural site in theNorth China Plain: mixed effects of urban plumesand biogenic emissions. J. Environ. Sci. (China) 71, 261–270.